

Discrete vector spatial solitons in a nonlinear waveguide array

Mark J. Ablowitz and Ziad H. Musslimani

Department of Applied Mathematics, University of Colorado, Campus Box 526, Boulder, Colorado 80309-0526

(Received 2 November 2001; published 21 May 2002)

A vector discrete diffraction managed soliton system is introduced. The vector model describes propagation of two polarization modes interacting in a nonlinear waveguide array with varying diffraction via the cross-phase modulation coupling. In the limit of strong diffraction we derive averaged equations governing the slow dynamics of the beam's amplitudes, and their stationary (in the form of bright-bright vector bound state) and traveling wave solutions are found. Through an extensive series of direct numerical simulations, interactions between diffraction-managed solitons for different values of velocities, diffraction, and cross-phase modulation coefficient are studied. We compare each collision case with its classical counterpart (constant diffraction) and find that in both the scalar and vector diffraction management cases, the interaction picture involves beam shaping, fusion, fission, nearly elastic collisions, and, in some cases, multihump structures. The collision scenario is found, in both the scalar and vector diffraction managed cases, to be rather different from the classical case.

DOI: 10.1103/PhysRevE.65.056618

PACS number(s): 42.65.Wi

I. INTRODUCTION

Recently, there has been considerable interest in the study of discrete spatial solitons in nonlinear media. Such solitons are localized modes of nonlinear lattices that form when discrete diffraction is balanced by nonlinearity. Discrete solitons have been demonstrated to exist in a wide range of physical systems; cf. Ref. [1]. An array of coupled optical waveguides is a setting that represents a convenient laboratory for experimental observations.

Discrete solitons in an optical waveguide array were theoretically predicted in [2]. Later on, many theoretical studies of discrete solitons in a waveguide array reported switching, steering, and other collision properties of these solitons [3,4] (see also the review papers [5]). In all of the above cases, the localized modes are solutions of the well-known discrete nonlinear Schrödinger (DNLS) equation that describes beam propagation in Kerr nonlinear media (according to coupled mode theory). However, discrete bright and dark solitons have also been found in quadratic media [6]. In some cases, their properties differ from their Kerr counterparts [7].

It took almost a decade until self-trapping of light in discrete nonlinear waveguide array was experimentally observed [8,9]. When a low intensity beam is injected into one or a few waveguides, the propagating field spreads over the adjacent waveguides, hence experiencing discrete diffraction. However, at sufficiently high power, the beam self-traps to form a localized state (a soliton) in the center waveguides. Subsequently, many interesting properties of nonlinear lattices and discrete solitons were reported. For example, the experimental observation of linear and nonlinear Bloch oscillations in AlGaAs waveguides [10], polymer waveguides [11], and in an array of curved optical waveguides [12]. Discrete systems have unique properties that are absent in continuous media such as the possibility of producing *anomalous* diffraction [13]. Hence, self-focusing and defocusing processes can be achieved in the same medium (structure) and wavelength. This also leads to the possibility of observing discrete dark solitons in self-focusing Kerr media [14].

The recent experimental observations of discrete solitons

[8] and diffraction management [13] have inspired further interest in discrete solitons in nonlinear lattices. This includes the newly proposed model of discrete diffraction managed nonlinear Schrödinger equation [15] whose width and peak amplitude vary periodically; optical spatial solitons in nonlinear photonic crystals [16] and the possibility of creating discrete solitons in Bose-Einstein condensation [17]. Also, very recently it was shown that discrete solitons in two-dimensional networks of nonlinear waveguides can be used to realize intelligent functional operations such as blocking, routing, logic functions, and time gating [18].

Here, we propose a vector discrete diffraction managed soliton system. The vector model describes propagation of two polarization modes interacting in a waveguide array with Kerr nonlinearity in the presence of varying diffraction. The coupling of the two fields is via the cross-phase modulation coefficient. In the limit of strong diffraction we derive averaged equations governing the slow dynamics of the beam's amplitudes. Stationary (in the form of bright-bright vector bound state) and traveling wave solutions are obtained. Through an extensive series of direct numerical simulations, we study interactions between periodic diffraction-managed solitons for different values of velocities, diffraction, and cross-phase modulation coefficient. In both the scalar and vector cases, we find that the interaction picture involves beam shaping, fusion, fission, nearly elastic collision, and, in some cases, multihump structures. The collision results, for the diffraction managed case, are often very different from their classical (constant diffraction) counterpart.

The paper is organized as follows. In Sec. II we set up a physical model that describes the propagation of two interacting optical fields in nonlinear waveguide array with varying diffraction. In Sec. III we discuss first the scalar limit of diffraction managed solitons. Section IV includes a derivation of the averaged equations that describe the slow dynamics of the beam's amplitude, followed in Sec. V by a discussion of the stationary solutions of a vector bright-bright bound state. Analysis of traveling wave solutions is discussed in Sec. VI. Different scenarios involving collisions between scalar and vector periodic diffraction-managed discrete solitons are presented in Sec. VII. Finally, we conclude in Sec. VIII.

II. MODEL DESCRIPTION

We begin our analysis by considering an infinite array of weakly coupled optical waveguides with equal separation d . The equation that governs the evolution of two interacting electric fields $E_n^{(1)}$ and $E_n^{(2)}$, according to nonlinear coupled mode theory [2,15,20,21], is given by

$$\frac{dE_n^{(j)}}{dz} = iC(E_{n+1}^{(j)} + E_{n-1}^{(j)}) + ik_w^{(j)}E_n^{(j)} + i(\boldsymbol{\kappa}\boldsymbol{\mathcal{E}}_n)_j E_n^{(j)},$$

$$j = 1, 2, \quad (1)$$

where $\boldsymbol{\kappa}$ is a 2×2 matrix with κ_{jj} and κ_{jl} , $j \neq l$ are the self- and cross-phase modulation coefficients, respectively, which result from the nonlinear index change; $\boldsymbol{\mathcal{E}}_n = (|E_n^{(1)}|^2, |E_n^{(2)}|^2)^T$, C is a coupling constant, z is the propagation distance, and $k_w^{(1,2)}$ are the propagation constants of the waveguides. When a cw mode of the form

$$E_n^{(1,2)}(z) = A_{1,2} \exp[i(k_x z - nk_x d)], \quad (2)$$

is inserted into the linearized version of Eqs. (1), it yields

$$k_z = k_w^{(1,2)} + 2C \cos(k_x d),$$

$$k_z'' = -2Cd^2 \cos(k_x d), \quad (3)$$

where in close analogy to the definition of dispersion, discrete diffraction is given by k_z'' . An important consequence of Eqs. (3) is that k_z'' can have a negative sign if $\pi/2 < |k_x d| \leq \pi$, hence, a light beam can experience anomalous diffraction. Experimentally, the sign and local value of the diffraction can be controlled and manipulated by launching light at a particular angle with respect to the normal to the waveguides or equivalently by tilting the waveguide array. To build a nonlinear model of diffraction management, we use a cascade of different segments of the waveguide, each piece being tilted by an angle zero and γ , respectively. The actual physical angle γ (the waveguide tilt angle) is related to the wave number k_x by the relation [13] $\sin \gamma = k_x/k$ where $k = 2\pi n_0/\lambda_0$ ($\lambda_0 = 1.53 \mu\text{m}$ is the central wavelength in vacuum and we take $n_0 = 3.3$ to be the linear refractive index). In this way, we generate a waveguide array with alternating diffraction. Next, we define the dimensionless amplitudes $U_n^{(j)}$ ($U_n^{(1)} \equiv U_n, U_n^{(2)} \equiv V_n$) by

$$E_n^{(j)} = \sqrt{P_*} U_n^{(j)} e^{i(k_w^{(j)} + 2C)z}, \quad z' = z/z_*, \quad (4)$$

where $P_* = \max(|U_n|_{\max}^2, |V_n|_{\max}^2)$ is the characteristic power and z_* is the nonlinear length scale. Substituting these quantities into Eqs. (1) yields the following (dropping the prime) diffraction-managed vector discrete nonlinear Schrödinger equations:

$$i \frac{dU_n}{dz} + \frac{D(z/z_w)}{2h^2} \delta_n^2 U_n + (|U_n|^2 + \eta |V_n|^2) U_n = 0,$$

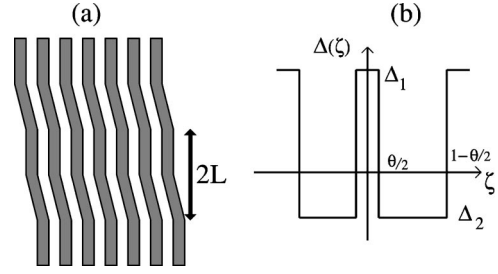


FIG. 1. Schematic presentation of the waveguide array (a) and of the diffraction map (b).

$$i \frac{dV_n}{dz} + \frac{D(z/z_w)}{2h^2} \delta_n^2 V_n + (\eta |U_n|^2 + |V_n|^2) V_n = 0, \quad (5)$$

with

$$\delta_n^2 A_n \equiv A_{n+1} + A_{n-1} - 2A_n, \quad (6)$$

where $\eta = \kappa_{12}/\kappa_{11}$ (we take $\kappa_{11} = \kappa_{22}$, $\kappa_{12} = \kappa_{21}$) and $z_* = 1/(\kappa_{11} P_*)$. We assume that $z_* C \cos(k_x d) = D(z/z_w)/(2h^2)$ where $D(z/z_w)$ is a piecewise constant periodic function that measures the local value of diffraction. Here $z_w \equiv 2L/z_*$ with L being the physical length of each waveguide segment [see Fig. 1(a) for a schematic representation]. Equations (5) describe the dynamical evolution of coupled beams in a Kerr medium with varying diffraction. When the “effective” nonlinearity balances the average diffraction then bright vector discrete solitons can form. The dependence of the coupling constant C on the waveguide width (ℓ) and separation (d) is given by (for AlGaAs waveguide) $C = (0.00984/\ell) \exp(-0.22d)$ (see Eq. 13.8-10 on pp. 523 of Ref. [19]). Therefore, the coupling constant C that corresponds to the experimental data reported in Ref. [14] (for $2.5 \mu\text{m}$ waveguide separation and width) is found to be $C = 2.27 \text{ mm}^{-1}$. For typical power $P_* \approx 300 \text{ W}$; typical nonlinear Kerr coefficient $\kappa_{11} = 3.6 \text{ m}^{-1} \text{ W}^{-1}$ and typical waveguide length $L \approx 100 \mu\text{m}$ we find $z_* \approx 1 \text{ mm}$ and $z_w \approx 0.2$, which suggests the use of asymptotic theory based on small z_w . Model (5) admits stationary soliton solution even when z_w is of order one. To this end, we consider here the case in which the diffraction takes the form

$$D(z/z_w) = \delta_a + \frac{1}{z_w} \Delta(z/z_w), \quad (7)$$

where δ_a is the average diffraction (taken to be positive) and $\Delta(z/z_w)$ is a periodic function [see Fig. 1(b)].

III. SCALAR CASE

In this section we review the scalar case, i.e., for which the cross-phase modulation coefficient vanishes ($\eta = 0$). In this case, Eq. (5) yields the following diffraction-managed DNLS (DM-DNLS) equation ($U_n = V_n \equiv \Phi_n$) [15]:

$$\frac{d\Phi_n}{dz} = i \frac{D(z/z_w)}{2h^2} \delta_n^2 \Phi_n + i |\Phi_n|^2 \Phi_n. \quad (8)$$

Since we are considering the case in which the diffraction changes rapidly ($z_w \ll 1$) and that Eq. (8) contains both slowly and rapidly varying terms, we introduce new fast and slow scales $\zeta = z/z_w$ and $Z = z$, respectively, and expand Φ_n in powers of z_w ,

$$\Phi_n = \Phi_n^{(0)}(\zeta, Z) + z_w \Phi_n^{(1)}(\zeta, Z) + O(z_w^2). \quad (9)$$

Substituting Eqs. (9) and (7) into Eq. (8) we find that the leading order in $1/z_w$ and the order 1 equations are, respectively, given by

$$\mathcal{L}(\Phi_n^{(0)}) = 0, \quad \mathcal{L}(\Phi_n^{(1)}) = -\mathcal{F}_n, \quad (10)$$

where

$$\mathcal{L}(A_n) \equiv i \frac{\partial A_n}{\partial \zeta} + \frac{\Delta(\zeta)}{2h^2} \delta_n^2 A_n, \quad (11)$$

and

$$\mathcal{F}_n = i \frac{\partial \Phi_n^{(0)}}{\partial Z} + \frac{\delta_a}{2h^2} \delta_n^2 \Phi_n^{(0)} + |\Phi_n^{(0)}|^2 \Phi_n^{(0)}.$$

To solve at order $1/z_w$, we introduce the *discrete* Fourier transform

$$\hat{w}(q, \zeta, Z) = \sum_{n=-\infty}^{+\infty} w_n(\zeta, Z) e^{-iqnh}, \quad (12)$$

with the inverse transform given by

$$w_n(\zeta, Z) = \frac{h}{2\pi} \int_{-\pi/h}^{\pi/h} \hat{w}(q, \zeta, Z) e^{iqnh} dq. \quad (13)$$

The solution is therefore given in the Fourier representation by ($\hat{\Phi}_0$ being the Fourier transform of $\Phi_n^{(0)}$)

$$\hat{\Phi}_0(q, \zeta, Z) = \hat{\varphi}(Z, q) \exp[-i\Omega(q)C(\zeta)], \quad (14)$$

with $\Omega(q) = [1 - \cos(qh)]/h^2$ and $C(\zeta) = \int_0^\zeta \Delta(\zeta') d\zeta'$. The amplitude $\hat{\varphi}(Z, q)$ is an arbitrary function whose dynamical evolution will be determined by a secularity condition associated with Eq. (10). In other words, the condition of the orthogonality of \mathcal{F}_n to all eigenfunctions χ_n of the adjoint homogeneous linear problem, which, when written in the Fourier domain, takes the form

$$\int_0^1 d\zeta \hat{\mathcal{F}}(q, \zeta, Z) \hat{\chi}(q, \zeta, Z) = 0, \quad (15)$$

where $\hat{\mathcal{F}}, \hat{\chi}$ are the Fourier transform of \mathcal{F}_n, χ_n , respectively. Here, $\hat{\mathcal{J}}^\dagger \hat{\chi} = 0$, with $\hat{\mathcal{J}}^\dagger$ being the adjoint operator to $\hat{\mathcal{L}} \equiv id/d\zeta - \Delta(\zeta)\Omega(q)$. Substituting Eq. (14) into $\hat{\mathcal{F}}$ using $\hat{\chi} = \exp[i\Omega(q)C(\zeta)]$ and performing the integration in condition (15) yields the following nonlinear evolution equation for $\hat{\varphi}(Z, q)$:

$$i \frac{d\hat{\varphi}(Z, q)}{dZ} = \delta_a \Omega(q) \hat{\varphi}(Z, q) - \mathcal{R}[\hat{\varphi}(Z, q)],$$

$$\mathcal{R} \equiv \int d\mathbf{q} \mathcal{K}(q, q_1, q_2) \hat{\varphi}(q_1) \hat{\varphi}(q_2) \hat{\varphi}^*(q_1 + q_2 - q), \quad (16)$$

where $d\mathbf{q} \equiv dq_1 dq_2$ and the kernel \mathcal{K} is defined by

$$\mathcal{K}(q, q_1, q_2) = \frac{h^2}{4\pi^2} \int_0^1 d\zeta \exp[iC(\zeta)\Lambda(q, q_1, q_2)],$$

$$\Lambda = \frac{4}{h^2} \cos\left(\frac{h(q_1 + q_2)}{2}\right) \prod_{j=1}^2 \sin\left(\frac{h(q_j - q)}{2}\right). \quad (17)$$

Equation (16) governs the evolution in Fourier space of a single optical beam in a coupled nonlinear waveguide array in the regime of strong diffraction. In the special case of two-step diffraction map shown in Fig. 1(b), i.e., when two waveguide segments are tilted by angle zero and γ alternatively, we have $\Delta(\zeta) = \Delta_1$ for $0 \leq |\zeta| < \theta/2$ and Δ_2 in the region $\theta/2 < |\zeta| < 1/2$, where θ is the fraction of the map with diffraction Δ_1 . In this case, the kernel \mathcal{K} takes the simple form

$$\mathcal{K} = \frac{h^2}{4\pi^2} \frac{\sin(s\Lambda)}{s\Lambda}, \quad (18)$$

with $s = [\theta\Delta_1 - (1 - \theta)\Delta_2]/4$. Importantly, these parameters can be related to the experiments reported in Ref. [13]. To achieve a waveguide configuration with alternate diffraction, we use two values of $k_x d = 0$ and $2\pi/3$ ($h = 1$), which correspond to waveguide tilt angles $\gamma = 0$ and 3.43° . In this case we find, for $\theta = 0.5$, $\Delta_1 = -\Delta_2 = 0.681$, $\delta_a = 1.135$ and $s = 0.17$. Different sets of parameters with a smaller angle γ are also realizable. Next, we look for a stationary solution for Eq. (16) (for the particular kernel given above) in the form $\hat{\varphi}(Z, q) = \hat{\varphi}_s(q) \exp(i\omega_s Z)$. Inserting this ansatz into Eq. (16) leads to

$$\hat{\varphi}_s(q) = \frac{1}{\delta_a \Omega(q) + \omega_s} \mathcal{R}[\hat{\varphi}_s(q)] \equiv \mathcal{Q}[\hat{\varphi}_s(q)], \quad (19)$$

which implies that the mode $\hat{\varphi}_s(q)$ is a fixed point of the nonlinear functional \mathcal{Q} . To numerically find the fixed point, we employ a modified Neumann iteration scheme [22–24] and write Eq. (19) in the form

$$\hat{\varphi}_s^{(m+1)}(q) = \left(\frac{s_L(\hat{\varphi}_s^{(m)})}{s_R(\hat{\varphi}_s^{(m)})} \right)^{3/2} \mathcal{Q}[\hat{\varphi}_s^{(m)}(q)], \quad m \geq 0,$$

$$s_L = \int |\hat{\varphi}_s^{(m)}(q)|^2 dq, \quad s_R = \int \hat{\varphi}_s^{(m)}(q) \mathcal{Q}[\hat{\varphi}_s^{(m)}(q)] dq.$$

The factors s_L and s_R are introduced to stabilize an otherwise divergent Neumann iteration scheme. This method is used to find stationary soliton solutions to the integral equation (16),

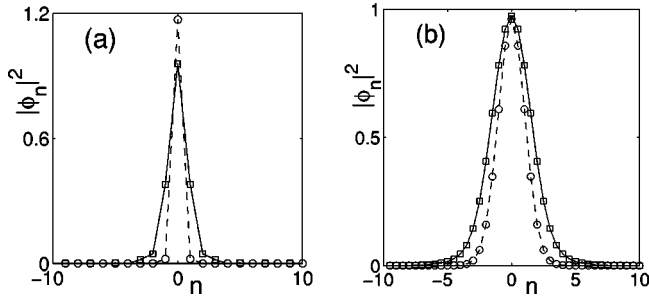


FIG. 2. Mode profile in physical space obtained from Eq. (19) (solid line) and from the average method (dashed line). Parameters are: (a) $\omega_s=1$, $h=1$, $s=0.17$, $\Delta_1=-\Delta_2=0.681$, $\delta_a=1.135$, and $z_w=0.2$; (b) $\omega_s=1$, $h=0.5$, $s=1$, $\Delta_1=-\Delta_2=4$, $\delta_a=1$, and $z_w=0.2$.

which in turn provides an asymptotic description of the diffraction-managed DNLS Eq. (8). It should also be noted that we can obtain periodic diffraction-compensated soliton solutions directly from Eq. (8). The technique is an alternative for finding periodic dispersion-managed solitons in communications problems [27–29]. The averaging procedure does not require that the map period, z_w , be small. To implement the method, initially we start with a guess, say $\varphi_n^{(0)} = \text{sech}(nh)$ with $\mathcal{E}_0 = \sum_{n=-\infty}^{\infty} \text{sech}^2(nh)$. Over one period this initial ansatz will evolve to $\varphi_n^{(0)'}$, which in general will have a chirp [30]. We then define an average:

$$\varphi_n^{(0)''} = \frac{1}{2} (\varphi_n^{(0)} + \varphi_n^{(0)'} \exp[-i\Theta_n]),$$

where $\varphi_n^{(0)'} = |\varphi_n^{(0)'}| \exp(i\Theta_n)$, which has power \mathcal{E}_0'' . Then $\varphi_n^{(1)} = \varphi_n^{(0)''} \sqrt{\mathcal{E}_0/\mathcal{E}_0''}$ is the new guess and in general the m th iteration takes the form

$$\varphi_n^{(m+1)} = \sqrt{\mathcal{E}_0/\mathcal{E}_m''} \varphi_n^{(m)''}, \quad \mathcal{E}_m'' = \sum_{n=-\infty}^{\infty} |\varphi_n^{(m)''}|^2. \quad (20)$$

In Fig. 2 the mode profiles associated with a stationary solution are depicted for two typical parameter values. The profiles are obtained by using both the integral equation approach as well as the averaged method. The evolutions of these discrete diffraction managed solitons are illustrated in Figs. 3 and 4 for the same two set of parameter values as in Fig. 2, respectively. We note that initially the beam has zero chirp [30]. During propagation a chirp develops and the peak

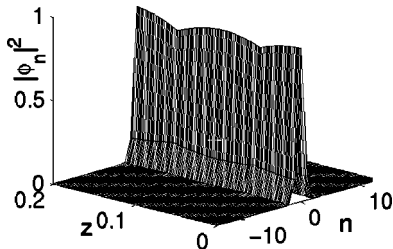


FIG. 3. Beam propagation over one period using Eq. (37) as initial condition obtained by a direct numerical simulation of Eq. (8). Parameters used are the same as in Fig. 2(a).

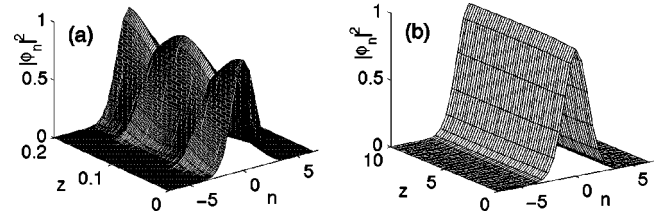


FIG. 4. Beam propagation over one period (a) and stationary evolution (b) obtained by a direct numerical simulation of Eq. (8) evaluated at end map period. Parameters used are the same as in Fig. 2(b).

amplitude of the beam begins to decrease and, as a result, the beam becomes wider (due to conservation of power). A full recovery of the soliton's initial amplitude and width is achieved at the end of the map period. This breathing behavior is shown in Figs. 3 and 4 for both strongly and moderately confined beams, respectively.

To establish the relation between the two approaches and to highlight the periodic nature of these new solitons, we calculate the nonlinear chirp by both the integral equation approach and the averaging method. It is clear that for small values of the map period, z_w , the asymptotic analysis is in good agreement with the averaging method, as shown in Fig. 5. We also mention briefly that the method of analysis associated with Eq. (8) can be modified to account for situations where the average diffraction is small, i.e., $\delta_a \ll 1$ and the local diffraction is $O(1)$. In such a situation we write $\delta_a = \epsilon D_a$, $D = \epsilon D_a + \Delta(z)$, $z = \xi/\epsilon$, and $\Phi_n = \sqrt{\epsilon} \Psi_n$. Then it is found that Ψ_n satisfies:

$$\frac{d\Psi_n}{d\xi} = i \frac{\mathcal{D}(\xi/\epsilon)}{2h^2} (\Psi_{n+1} + \Psi_{n-1} - 2\Psi_n) + i |\Psi_n|^2 \Psi_n, \quad (21)$$

where $\mathcal{D}(\xi/\epsilon) = D_a + (1/\epsilon)\Delta(\xi/\epsilon)$. The model (21) is valid in parameter regimes, which applies to a physical situation where the average diffraction is small and local diffraction is of order one.

IV. VECTOR CASE: AVERAGED EQUATIONS

In this section we will discuss the full vector system (5) in the limit of strong diffraction. Following Sec. III we again expand the fields U_n , V_n in powers of z_w ,

$$\begin{aligned} U_n &= U_n^{(0)}(\zeta, Z) + z_w U_n^{(1)}(\zeta, Z) + O(z_w^2), \\ V_n &= V_n^{(0)}(\zeta, Z) + z_w V_n^{(1)}(\zeta, Z) + O(z_w^2). \end{aligned} \quad (22)$$

Substituting Eqs. (22) and (7) into Eqs. (5) we find that at leading order [$O(1/z_w)$],

$$\mathcal{L}(U_n^{(0)}) = 0, \quad \mathcal{L}(V_n^{(0)}) = 0, \quad (23)$$

while the order 1 equations are

$$\mathcal{L}(U_n^{(1)}) = -\mathcal{G}_n^{(1)}, \quad \mathcal{L}(V_n^{(1)}) = -\mathcal{G}_n^{(2)}, \quad (24)$$

where the linear operator \mathcal{L} is given in Eq. (11) and

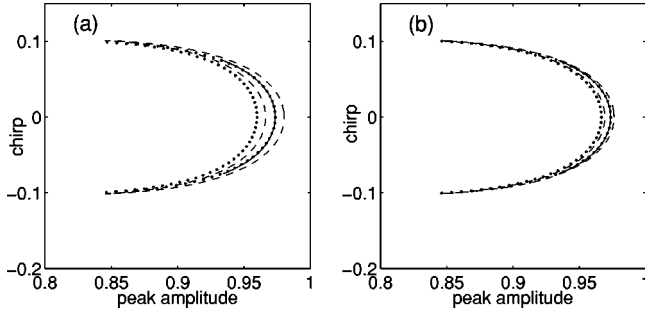


FIG. 5. Periodic evolution of the beam chirp versus maximum peak power. Solid line represents the leading order approximation, i.e., Eq. (14); dashed line represents numerical solution of the DM-DNLS, and dotted line depicts the evolution of the leading order solution under Eq. (8). Parameters used are the same as in Fig. 2(b) with $z_w = 0.2$ (a) and 0.1 (b).

$$\mathcal{G}_n^{(1)} = i \frac{\partial U_n^{(0)}}{\partial Z} + \frac{\delta_a}{2h^2} \delta_n^2 U_n^{(0)} + (|U_n^{(0)}|^2 + \eta |V_n^{(0)}|^2) U_n^{(0)},$$

$$\mathcal{G}_n^{(2)} = i \frac{\partial V_n^{(0)}}{\partial Z} + \frac{\delta_a}{2h^2} \delta_n^2 V_n^{(0)} + (\eta |U_n^{(0)}|^2 + |V_n^{(0)}|^2) V_n^{(0)}.$$

To solve at order $1/z_w$, we make use of the discrete Fourier transform (12). The solution to Eqs. (23) is thus given in the Fourier representation by

$$\hat{U}_0 = \hat{\psi}(Z, q) e^{-i\Omega(q)C(\zeta)}, \quad \hat{V}_0 = \hat{\phi}(Z, q) e^{-i\Omega(q)C(\zeta)}, \quad (25)$$

where \hat{U}_0, \hat{V}_0 are the Fourier transforms of $U_n^{(0)}$ and $V_n^{(0)}$. The amplitudes $\hat{\psi}$ and $\hat{\phi}$ are arbitrary functions whose dynamical evolution will be determined by a secularity condition associated with Eqs. (24). In other words, the condition of the orthogonality of $\mathcal{G}_n^{(1,2)}$ to all eigenfunctions χ_n of the homogeneous adjoint linear problem that, when written in the Fourier domain, takes the form

$$\int_0^1 d\zeta \hat{\mathcal{G}}^{(1,2)}(q, \zeta, Z) \hat{\chi}(q, \zeta, Z) = 0, \quad (26)$$

where $\hat{\mathcal{G}}^{(1,2)}, \hat{\chi}$ are the Fourier transforms of $\mathcal{G}_n^{(1,2)}$ and χ_n , respectively; $\hat{\chi}$ satisfies $\hat{\mathcal{L}}^\dagger \hat{\chi} = 0$ with $\hat{\mathcal{L}}^\dagger$ being the adjoint operator to $\hat{\mathcal{L}} \equiv i(\partial/\partial\zeta) - \Delta(\zeta)\Omega(q)$. Substituting Eq. (25) into $\hat{\mathcal{G}}^{(1,2)}$ and performing the integration in condition (26) with $\hat{\chi} = \exp[i\Omega(q)C(\zeta)]$ yields the following coupled nonlinear evolution equations for the amplitudes $\hat{\psi}$ and $\hat{\phi}$:

$$\begin{aligned} i \frac{d\hat{\psi}(Z, q)}{dZ} &= \delta_a \Omega(q) \hat{\psi}(Z, q) - \mathcal{A}[\hat{\psi}, \hat{\phi}], \\ i \frac{d\hat{\phi}(Z, q)}{dZ} &= \delta_a \Omega(q) \hat{\phi}(Z, q) - \mathcal{B}[\hat{\psi}, \hat{\phi}], \end{aligned} \quad (27)$$

with

$$\begin{aligned} \mathcal{A} &= \int d\mathbf{q} \mathcal{K}(q, q_1, q_2) [\hat{\psi}(q_1) \hat{\psi}(q_2) \hat{\psi}^*(q_1 + q_2 - q) \\ &\quad + \eta \hat{\phi}(q_1) \hat{\psi}(q_2) \hat{\phi}^*(q_1 + q_2 - q)], \\ \mathcal{B} &= \int d\mathbf{q} \mathcal{K}(q, q_1, q_2) [\hat{\phi}(q_1) \hat{\phi}(q_2) \hat{\phi}^*(q_1 + q_2 - q) \\ &\quad + \eta \hat{\psi}(q_1) \hat{\phi}(q_2) \hat{\psi}^*(q_1 + q_2 - q)], \end{aligned}$$

where as before $d\mathbf{q} \equiv dq_1 dq_2$ and the kernel \mathcal{K} is given by Eq. (17). Equations (27) govern the averaged evolution (in Fourier space) of coupled optical beams in a nonlinear waveguide array in the regime of strong diffraction. The above results are general and hold for any diffraction map. However, the analysis simplifies significantly in the special case of two-step diffraction map shown in Fig. 1(b), in which case the kernel is given by Eq. (18).

V. STATIONARY SOLUTIONS

We now look for a stationary solution for Eqs. (27) [for the particular kernel given in Eq. (18)] in the form

$$\hat{\psi}(Z, q) = \hat{\psi}_s e^{i\mu Z}, \quad \hat{\phi}(Z, q) = \hat{\phi}_s e^{i\nu Z}. \quad (28)$$

Inserting this ansatz into Eq. (27) leads to

$$\begin{aligned} \hat{\psi}_s(q) &= \mathcal{A}[\delta_a \Omega(q) + \mu] \equiv \mathcal{M}, \\ \hat{\phi}_s(q) &= \mathcal{B}[\delta_a \Omega(q) + \nu] \equiv \mathcal{N}. \end{aligned} \quad (29)$$

To numerically find the modes $\hat{\psi}_s(q)$ and $\hat{\phi}_s(q)$, we employ the modified Neumann iteration scheme mentioned in Sec. III and write Eqs. (29) in the form

$$\hat{\psi}_s^{(m+1)} = \left(\frac{s_L^{(1)}}{s_R^{(1)}} \right)^\alpha \mathcal{M}_m, \quad \hat{\phi}_s^{(m+1)} = \left(\frac{s_L^{(2)}}{s_R^{(2)}} \right)^\alpha \mathcal{N}_m, \quad (30)$$

$$s_L^{(1)} = \int |\hat{\psi}_s^{(m)}|^2 dq, \quad s_L^{(2)} = \int |\hat{\phi}_s^{(m)}|^2 dq,$$

$$s_R^{(1)} = \int \hat{\psi}_s^{(m)} \mathcal{M}_m dq, \quad s_R^{(2)} = \int \hat{\phi}_s^{(m)} \mathcal{N}_m dq.$$

The factor $\alpha = 3/2$ is chosen to make the right-hand side of Eqs. (30) of degree zero, which yields convergence of the scheme [22,23]. Clearly, when $\hat{\psi}_s^{(m)}(q) \rightarrow \hat{\psi}_s(q)$, $\hat{\phi}_s^{(m)}(q) \rightarrow \hat{\phi}_s(q)$ as $m \rightarrow \infty$ then $s_L^{(1)}/s_R^{(1)} \rightarrow 1$, $s_L^{(2)}/s_R^{(2)} \rightarrow 1$ and in turn $\hat{\phi}_s(q)$, $\hat{\psi}_s(q)$ will be the solutions to Eqs. (29). The factors $s_L^{(j)}$ and $s_R^{(j)}$, $j=1,2$ are introduced to stabilize an otherwise divergent simple Neumann iteration scheme. Note that when applying the continuous Fourier transform to find stationary solutions, the numerical scheme based on Eq. (30) does not converge which indicates that, contrary to the vector integrable DNLS [25,26], continuous stationary solutions may not exist. Figures 6,7 show typical solutions to Eq. (29) both in the Fourier domain (Fig. 6) and in physical space

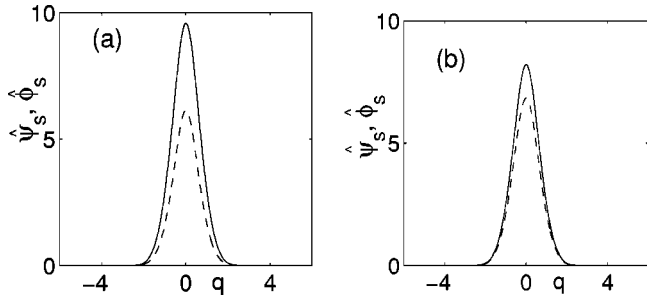


FIG. 6. Mode profiles, $\hat{\psi}_s$ (solid line) and $\hat{\phi}_s$ (dashed line) in the Fourier space obtained from Eqs. (30). Parameters are $\omega_s=1$, $h=0.5$, $s=1$, $\Delta_1=-\Delta_2=4$, $\delta_a=1$, and $z_w=0.2$. (a) $\eta=2/3$ and (b) $\eta=1$.

(Fig. 7) for lattice spacing $h=0.5$. The evolution of these discrete diffraction managed solitons is illustrated in Fig. 8 for the same set of parameter values as in Fig. 6. We note that initially the vector solitons have zero chirp. During propagation a chirp develops and the peak amplitude of each beam begins to decrease and, as a result, the two beams become wider (due to conservation of power). A full recovery of the vector soliton's initial amplitudes and widths is achieved at the end of the map period. This breathing behavior is shown in Fig. 8 for different values of cross-phase modulation (η). Finally, in Fig. 9 we show the stationary evolution of these beams evaluated at each map period.

VI. TRAVELING SOLITONS

In this section we will discuss traveling wave solution to Eqs. (5) in the limit of strong diffraction management. With soliton collisions in mind we consider here the case where the two interacting beams are initially well separated, in which case, the overlap terms $|V_n|^2 U_n$ and $|U_n|^2 V_n$ are very small compared to the self-phase modulation term. Therefore, in what follows we find travelling wave solutions in the case $\eta=0$, i.e., in the scalar diffraction managed model. Our approach can be generalized to the $\eta \neq 0$ case for which the two polarizations travel possibly at different speed. We look for a traveling wave solution in the form

$$U_n(z) = u(\xi, z) e^{-i\varphi_n}, \quad \xi = nh - V \int_0^z D, \quad (31)$$

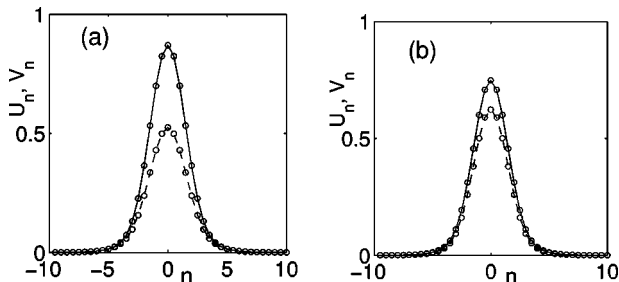


FIG. 7. Mode profiles, U_n (solid line) and V_n (dashed line) in physical space. Parameters are the same as in Fig. 6 with $\eta=2/3$ (a) and 1 (b). Circles denote grid points.

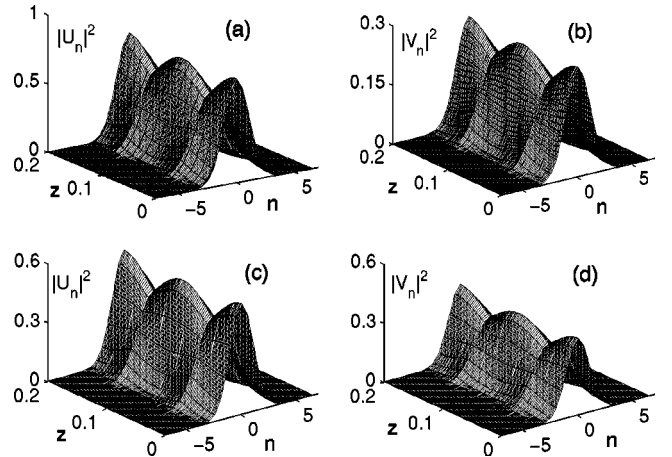


FIG. 8. Beam propagation over one period using Eq. (25) as initial conditions obtained by a direct numerical simulation of Eqs. (5). Parameters used are the same as in Fig. 6 with $\eta=2/3$ (a), (b) and $\eta=1$ (c), (d).

with $\varphi_n = \beta n h - \omega \int_0^z D$. Note that we allow the amplitude u to depend explicitly on z . The reason is that when the diffraction is constant ($D=D_0=\text{const}$) and the amplitude u is independent of z , then the problem reduces to finding traveling wave solution to the DNLS equation [31–36]. However, recent studies [24] of traveling solitons of the DNLS equation reveal the important conclusion that a uniformly moving continuous wave solution is unlikely to exist. These results differ from those of Ref. [31] in which “continuous” traveling solitary waves were reported using Fourier series expansions with finite period L while *assuming convergence* as $L \rightarrow \infty$. Even then, for moderately localized pulses, “approximate” traveling waves are found to persist for long distances without radiation. However, for strongly localized beams, the wave front gets distorted during propagation and it decelerates. Nevertheless, the pulse travels almost uniformly over the experimental distance (6 mm).

Mathematically, we analyze the problem as follows. Substituting Eq. (31) into Eq. (5) leads to

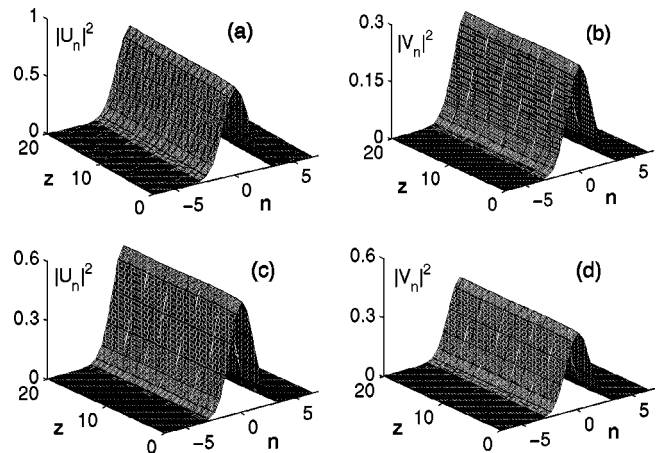


FIG. 9. Stationary evolution obtained by a direct numerical simulation of Eqs. (5) evaluated at end map period. Parameters used are the same as in Fig. 6 with $\eta=2/3$ (a), (b) and $\eta=1$ (c), (d).

$$i\frac{\partial u}{\partial z} = D(z/z_w) \left(iV \frac{\partial u}{\partial \xi} - \frac{T_\beta u}{2h^2} + \omega u \right) - |u|^2 u, \quad (32)$$

where $D(z/z_w)$ is the diffraction function given in Eq. (7) and

$$T_\beta u \equiv e^{-i\beta h} u(\xi+h) + e^{i\beta h} u(\xi-h) - 2u(\xi).$$

Since in this case, Eq. (32) contains both slowly and rapidly varying terms, we proceed as before and define new fast and slow scales $\zeta = z/z_w$ and $Z = z$, respectively, and expand u in powers of z_w ,

$$u(\xi, z) = u_0(\zeta, \xi, Z) + z_w u_1(\zeta, \xi, Z) + O(z_w^2). \quad (33)$$

Substituting Eq. (33) into (32) we find that the leading order [$O(1/z_w)$] and the order 1 equations are, respectively, given by

$$\mathcal{J}(u_0) = 0, \quad \mathcal{J}(u_1) = -\mathcal{U}, \quad (34)$$

where

$$\mathcal{J}(A) \equiv i \frac{\partial A}{\partial \zeta} - iV \Delta(\zeta) \frac{\partial A}{\partial \xi} - \omega \Delta(\zeta) A + \frac{\Delta(\zeta)}{2h^2} T_\beta A,$$

$$\mathcal{U} \equiv i \frac{\partial u_0}{\partial Z} - \delta_a \left(iV \frac{\partial u_0}{\partial \xi} - \frac{T_\beta u_0}{2h^2} + \omega u_0 \right) + |u_0|^2 u_0.$$

To solve at order $1/z_w$, we again introduce the *discrete* Fourier transform (treating ξ as a discrete variable)

$$\begin{aligned} \hat{u}_0(q, \zeta, Z) &= \sum_{\xi = m h \in \mathbf{Z}} u_0(\zeta, \xi, Z) e^{-iq\xi}, \\ u_0(\zeta, \xi, Z) &= \frac{h}{2\pi} \int_{-\pi/h}^{\pi/h} \hat{u}_0(q, \zeta, Z) e^{iq\xi} dq. \end{aligned} \quad (35)$$

At this stage it is useful to make some further comments on the Fourier transform. Since ξ is a continuous variable it implies that Eq. (32) is a continuous equation in both ξ and z . Therefore it seems natural to solve Eqs. (34) using the *continuous* Fourier transform given by

$$\begin{aligned} \hat{u}_0(q, \zeta, Z) &= \int_{-\infty}^{\infty} u_0(\zeta, \xi, Z) e^{-iq\xi} d\xi, \\ u_0(\zeta, \xi, Z) &= \frac{1}{2\pi} \int_{-\infty}^{\infty} \hat{u}_0(q, \zeta, Z) e^{iq\xi} dq. \end{aligned} \quad (36)$$

But when applying the continuous Fourier transform, our numerical scheme fails to converge [24]. However, when we use the discrete Fourier transform our method yields an approximate but *not* exact solution. The solution at $O(1/z_w)$ is given in the Fourier representation by

$$\hat{u}_0(q, \zeta, Z) = \hat{U}(Z, q) \exp[-iS(q, \beta)C(\zeta)], \quad (37)$$

with $S(q, \beta) = \omega - qV + \{1 - \cos[(q - \beta)h]\}/h^2$. As in Sec. III the amplitude $\hat{U}(Z, q)$ is an arbitrary function whose dynamical evolution is determined by a secularity condition associated with the order 1 equation. In other words, the condition of the orthogonality of \mathcal{U} to all eigenfunctions χ_β of the adjoint linear problem, which, when written in the Fourier domain, takes the form

$$\int_0^1 d\zeta \hat{\mathcal{U}}(q, \zeta, Z) \hat{\chi}_\beta(q, \zeta, Z) = 0, \quad (38)$$

where $\hat{\mathcal{U}}, \hat{\chi}_\beta$ are the Fourier transform of \mathcal{U}, χ_β respectively. Here, $\hat{\mathcal{J}}^\dagger \hat{\chi}_\beta = 0$ with $\hat{\mathcal{J}}^\dagger$ being the adjoint operator to $\hat{\mathcal{J}} \equiv id/d\zeta - \Delta(\zeta)S(q, \beta)$. Substituting Eq. (37) into $\hat{\mathcal{U}}$ using $\hat{\chi}_\beta = \exp[iS(q, \beta)C(\zeta)]$ and performing the integration in condition (38) yields the following nonlinear evolution equation for $\hat{U}(Z, q)$:

$$\begin{aligned} i \frac{d\hat{U}(Z, q)}{dZ} - \delta_a S(q, \beta) \hat{U}(Z, q) + \mathcal{P}[\hat{U}(Z, q)] &= 0, \\ \mathcal{P} &\equiv \int d\mathbf{q} \mathcal{K}_\beta(q, q_1, q_2) \hat{U}(q_1) \hat{U}(q_2) \hat{U}^*(q_1 + q_2 - q), \end{aligned} \quad (39)$$

where $d\mathbf{q} \equiv dq_1 dq_2$ and the kernel \mathcal{K}_β is defined by

$$\begin{aligned} \mathcal{K}_\beta(q, q_1, q_2) &= \frac{h^2}{4\pi^2} \int_0^1 d\zeta \exp[iC(\zeta)\Lambda_\beta(q, q_1, q_2)], \\ \Lambda_\beta &= \frac{4}{h^2} \cos\left(\frac{h(q_1 + q_2 - 2\beta)}{2}\right) \prod_{j=1}^2 \sin\left(\frac{h(q_j - q)}{2}\right). \end{aligned}$$

Restricting the discussion to the two-step diffraction map (see Fig. 1 and Sec. III), we find $\mathcal{K}_\beta = h^2 \sin(s\Lambda_\beta)/(4\pi^2 s\Lambda_\beta)$. To find a moving solitary wave solution to system (39), we write

$$\hat{U}(Z, q) = \hat{U}_{\text{TW}}(q) e^{i\omega Z} = [\hat{U}_e(q) + \hat{U}_o(q)] e^{i\omega Z}, \quad (40)$$

with $\hat{U}_e(q)$ and $\hat{U}_o(q)$ being the even and odd parts of $\hat{U}_{\text{TW}}(q)$. This choice of ansatz is consistent with the problem of finding traveling solitary waves for the DNLS equation (constant diffraction) where it was shown [24] that the mode profile in physical space can be written as $U = [F(\xi) + iG(\xi)] \exp[\beta nh - \omega z]$ with F, G being even and odd functions, respectively. Substituting Eq. (40) into Eq. (39) we arrive at

$$\hat{U}_{\text{TW}}^{(m+1)}(q) = \left(\frac{s_L}{s_R}\right)^{3/2} \frac{\mathcal{P}[\hat{U}_{\text{TW}}^{(m)}(q)]}{\omega + \delta_a S(q, \beta)}, \quad (41)$$

where s_L and s_R are the convergence factors introduced in Sec. III. For a given set of parameters h, ω , and $\beta > 0$, the mode shapes and soliton velocity are found by iterating Eq. (41) with an initial guess, e.g., $\hat{U}_e^{(0)}(q) = \text{sech}(q)$, $\hat{U}_o^{(0)}(q) = \text{sech}(q) \tanh(q)$, and $V = V_* < 0$. The iterations are carried

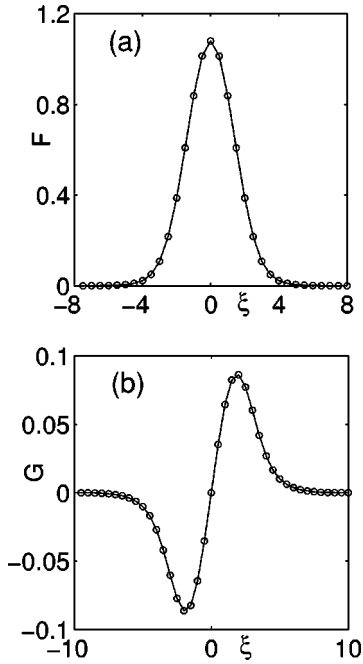


FIG. 10. Traveling wave solution to Eq. (39) in real space. (a) shows the even part and (b) the odd part. Parameters are $s=1$, $\Delta_1=-\Delta_2=4$, $\delta_a=1$, $z_w=0.1$, $\omega=1$, $h=0.5$, $\beta=0.5$, and $V=-0.5$. Circles denote grid points.

out until the condition $|s_L - s_R| < \epsilon$ is satisfied with $\epsilon > 0$ being a prescribed tolerance. However, unlike the stationary case, here, the soliton velocity is still to be determined. For any choice of $V_* < 0$ if $|s_L - s_R| < \epsilon$, we seek a different value of V_* at which $s_L - s_R$ changes sign. Then, we use the bisection method to change V_* in order to locate the correct velocity V and modes \hat{U}_e , \hat{U}_o for each ω , β , and h . A typical soliton mode is shown in Fig. 10 for velocity $V=-0.5$ and lattice spacing $h=0.5$.

VII. COLLISIONS BETWEEN DISCRETE SOLITONS

Having found a moving discrete diffraction managed solitary wave we next study interactions between them [Fig. 11]. We have conducted a series of numerical simulations both in the scalar (for different soliton velocities) and vector (for different values of the cross-phase modulation coefficient and different velocities). Below we discuss each case separately. To keep the paper self-contained, we consider first interactions between scalar and vector discrete solitary waves in the case of constant diffraction, i.e., when Δ_1 and Δ_2 are both zero ($s=0$), which implies constant kernel $\mathcal{K} = h^2/4\pi^2$.

A. Scalar interaction: Constant diffraction

Scalar discrete excitations propagating in a media with normal diffraction are solutions of the DNLS equation [see Eq. (8) with constant $D(z/z_w) \equiv 1$]:

$$\frac{dW_n}{dz} = \frac{i}{2h^2} \delta_n^2 W_n + i |W_n|^2 W_n. \quad (42)$$

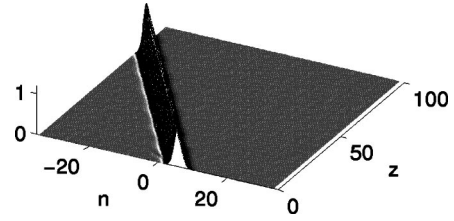


FIG. 11. Evolution of a moderately localized soliton in physical domain obtained by a direct numerical simulation of Eq. (8) evaluated at end map period. Parameters are $s=1$, $\Delta_1=-\Delta_2=4$, $\delta_a=1$, $z_w=0.1$, $\omega=1$, $h=0.5$, $\beta=0.5$, and $V=-0.5$. Shown on the vertical axis is the beam intensity $|U_n|^2$.

To simulate the collision process between discrete solitons we first need to obtain a traveling wave solution to the above equation. To do so, we look for traveling localized modes in the form

$$W_n(z) = w(\xi) \exp(-i\beta n h + i\omega z), \quad (43)$$

with $\xi = n h - V z$ where V and ω are the soliton velocity and wave number shift, respectively. Assuming w is complex, i.e., $w(\xi) = w_R(\xi) + i w_I(\xi)$ then Eq. (42) takes the form

$$\begin{aligned} V w_I' + \Xi_1 w_R + \Xi_2 w_I + (w_R^2 + w_I^2) w_R &= \omega w_R, \\ -V w_R' + \Xi_1 w_I - \Xi_2 w_R + (w_R^2 + w_I^2) w_I &= \omega w_I, \end{aligned} \quad (44)$$

where prime denotes derivative with respect to ξ and

$$\begin{aligned} \Xi_1 X &= \frac{1}{h^2} [\cos(\beta h)(E_+ + E_-)X - 2X], \\ \Xi_2 X &= \frac{\sin(\beta h)}{h^2} (E_+ - E_-)X, \end{aligned} \quad (45)$$

with $E_{\pm} X(\xi) \equiv X(\xi \pm h)$. Note that system (44) is invariant under the transformation: $\beta \rightarrow -\beta$, $w_I \rightarrow -w_I$, and $V \rightarrow -V$, which will play a central role in collision processes. To find the mode shapes and soliton velocity, we proceed as before by taking the discrete Fourier transform of Eqs. (44), which yields the following iteration scheme:

$$\begin{aligned} \hat{w}_R^{(m+1)}(q) &= \frac{\Omega_2(q)}{\Omega_1(q)} \tilde{w}_I^{(m)}(q) + (s_L^{(1)}/s_R^{(1)})^{3/2} \mathcal{I}_1, \\ \tilde{w}_I^{(m+1)}(q) &= \frac{\Omega_2(q)}{\Omega_1(q)} \hat{w}_R^{(m)}(q) + (s_L^{(2)}/s_R^{(2)})^{3/2} \mathcal{I}_2, \end{aligned} \quad (46)$$

where $\hat{w}_R(q)$ and $\hat{w}_I(q) \equiv -i \tilde{w}_I(q)$ are the Fourier transforms of $w_R(\xi)$ and $w_I(\xi)$, respectively, and

$$\begin{aligned} \mathcal{I}_1 &= \frac{h^2}{4\pi^2 \Omega_1(q)} (\hat{w}_R * \hat{w}_R * \hat{w}_R - \tilde{w}_I * \tilde{w}_I * \hat{w}_R), \\ \mathcal{I}_2 &= \frac{h^2}{4\pi^2 \Omega_1(q)} (\hat{w}_R * \hat{w}_R * \tilde{w}_I - \tilde{w}_I * \tilde{w}_I * \tilde{w}_I). \end{aligned} \quad (47)$$

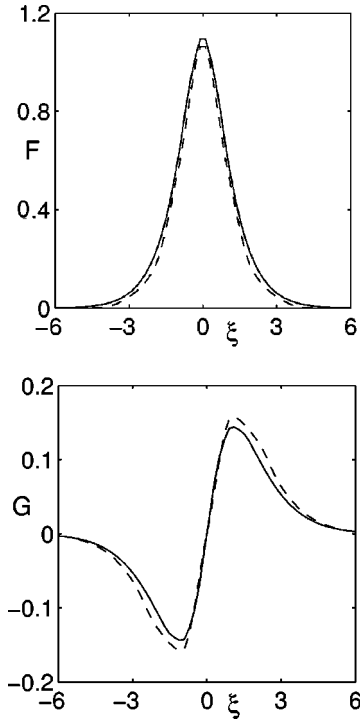


FIG. 12. Mode shapes in physical space for $\omega=1$ and $\beta=0.5$. Solid line corresponds to $h=0.5$ and velocity $V=-0.5$, whereas dashed line for $h=1$ and $V=-0.3$.

The convergence factors $s_L^{(j)}$ and $s_R^{(j)}$, $j=1,2$ are

$$s_L^{(1)} = \int \hat{w}_R^{(m)}(q) \left(\hat{w}_R^{(m)}(q) - \frac{\Omega_2(q)}{\Omega_1(q)} \tilde{w}_I^{(m)}(q) \right) dq,$$

$$s_R^{(1)} = \int \hat{w}_R^{(m)}(q) \mathcal{I}_1 dq, \quad s_R^{(2)} = \int \tilde{w}_I^{(m)}(q) \mathcal{I}_2 dq, \quad (48)$$

and $s_L^{(2)}$ is obtained from $s_L^{(1)}$ by interchanging \hat{w}_R and \tilde{w}_I . Here, $\Omega_1(q) = \omega + (2/h^2)[1 - \cos(hq)\cos(\beta h)]$ and $\Omega_2(q) = (2/h^2)\sin(hq)\sin(\beta h) + Vq$. For a given set of parameters h , ω , and $\beta > 0$, the mode shapes and soliton velocity are found by iterating system (46) together with the bisection technique outlined in Sec. VI. Typical traveling soliton modes are shown in Fig. 12. Having obtained moving solitary wave solutions, we investigated next the collision process. If the soliton speed is less than a critical velocity, $|V| < V_c \approx 0.2$, then the solitons are found to fuse after collision accompanied with radiation modes, see Figs. 13(a), 13(b). However, when the two modes move sufficiently fast ($V > V_c$) then they pass through each other. This collision results in two “nonstationary” travelling waves moving in the opposite directions with modulated envelopes [Fig. 13(c)].

B. Vector interaction: Constant diffraction

The vector discrete system with constant diffraction is described by the following coupled discrete NLS equations

$$i \frac{dU_n}{dz} + \frac{1}{2h^2} \delta_n^2 U_n + (|U_n|^2 + \eta |V_n|^2) U_n = 0,$$

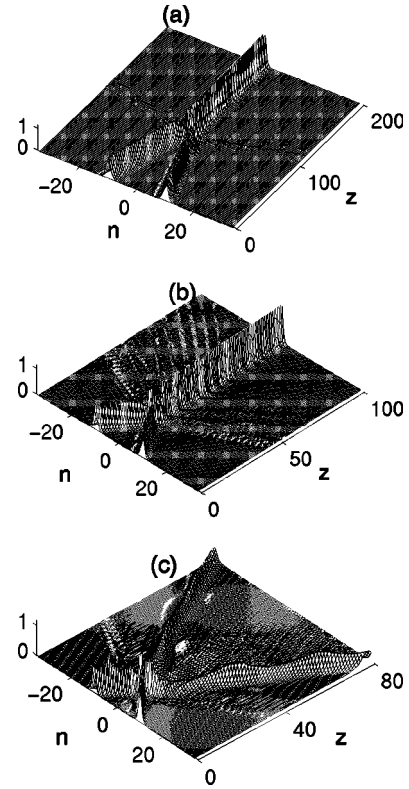


FIG. 13. Interaction between scalar “classical” discrete solitons for different values of velocity obtained by a direct numerical simulation of Eq. (42). Parameters are $h=0.5$, and $V = \mp 0.1$, $\beta = \pm 0.1$ (a); $V = \mp 0.25$, $\beta = \pm 0.25$ (b); and $V = \mp 0.5$, $\beta = \pm 0.5$ (c). Shown on the vertical axis is the intensity $|W_n|^2$

$$i \frac{dV_n}{dz} + \frac{1}{2h^2} \delta_n^2 V_n + (\eta |U_n|^2 + |V_n|^2) V_n = 0, \quad (49)$$

where U_n , V_n are the two interacting beams and η is the cross-phase modulation coefficient. To study interaction between vector solitons, we consider the case in which the two modes are initially well separated and orthogonally polarized. In this situation, the two modes are completely decoupled and each one of them satisfies a scalar DNLS equation for which a traveling solitary wave was obtained in the preceding section. In Fig. 14 we show a typical collision experiment for different values of cross-phase modulation coefficient and different soliton velocities. In all cases the U_n mode is always stationary while the other one moves with speed V . When $\eta = 2/3$ and the second mode (V_n) moves slowly ($V = -0.1$), we observe power exchange [see Fig. 14(a) and Fig. 15(a)], i.e., the outgoing beams have amplitudes different from the one before the collision. The V_n field mostly survived the collision whereas U_n undergoes a fission process and two solitons are born. Each one of them has amplitude almost half the original one. The interaction picture is more “clean” at higher speed ($V = -0.4$) in which the two modes pass each other nearly unaffected [except for a phase shift in the soliton position, Fig. 14(b) and Fig. 15(b)]. Decreasing the value of η to 0.5 leads to a different picture. In this case when $V = -0.1$ the two beams fuse [see Fig. 14(c) and Fig. 15(c)] and form a single fused traveling wave

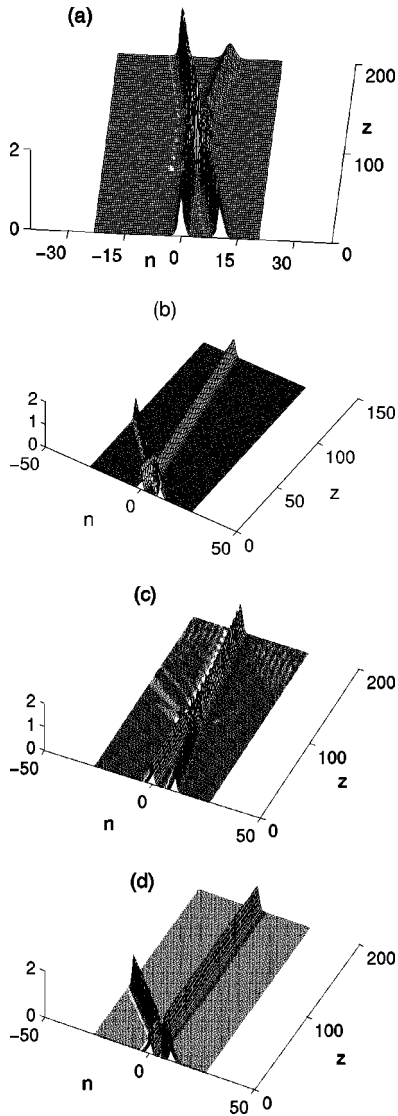


FIG. 14. Interaction between discrete “classical” vector solitons for different values of cross-phase modulation coefficient η and different soliton velocity. Shown on the vertical axis is the intensity of the two colliding beams, i.e., $I_n = |U_n|^2 + |V_n|^2$. Before collision, U_n is the left beam, whereas V_n is the right beam. In all the parts, the incoming U_n mode is stationary, whereas V_n travels with a speed V . Parameters used are $\eta=2/3$, $V=-0.1$, $\beta=0.1$ (a); $\eta=2/3$, $V=-0.4$, $\beta=0.4$ (b); $\eta=0.5$, $V=-0.1$, $\beta=0.1$ (c); and $\eta=1$, $V=-0.5$, $\beta=0.5$ (d).

whereas the two modes simply go through each other at higher velocity ($V=-0.5$) as shown in Fig. 14(d) and Fig. 15(d). Notice that the collision process reported in Fig. 15(d) is nearly elastic. Unlike the symmetric discrete vector NLS equation, where the nonlinear terms are taken to be $(|U_n|^2 + \eta|V_n|^2)(U_{n+1} + U_{n-1})$ and $(\eta|U_n|^2 + |V_n|^2)(V_{n+1} + V_{n-1})$ [25], here (vector nonintegrable case), we did not find a bouncing process. This could be attributed to the special properties of the symmetric vector NLS system.

C. Scalar interaction: Diffraction management

In this section we study interactions between scalar discrete diffraction managed solitons. In what follows, we high-

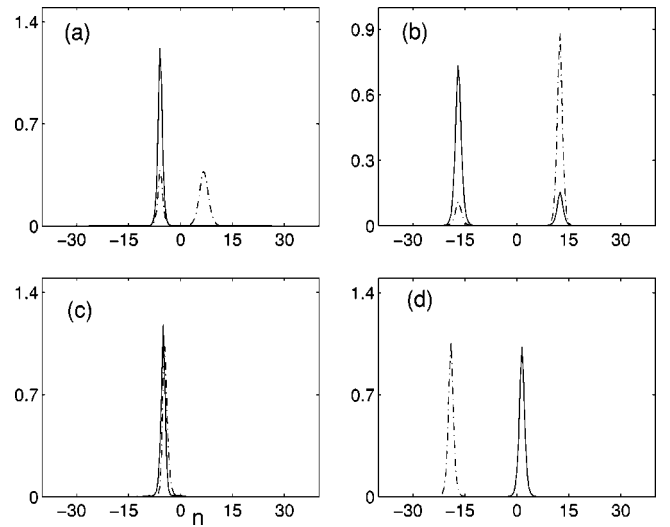


FIG. 15. Snapshot showing the final state of the collision illustrated in Fig. 14. (a)–(d) correspond to Figs. 14(a)–14(d), respectively. Dashed (solid) line corresponds to U_n (V_n).

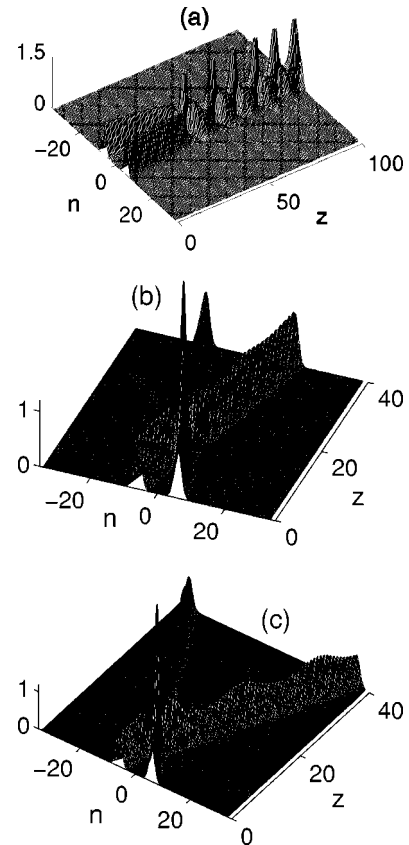


FIG. 16. Interaction between scalar diffraction-managed solitons for different values of velocity obtained by a direct numerical simulation of Eq. (8) evaluated at end map period. Parameters are $\omega=1$, $h=0.5$, $s=1$, $\Delta_1=-\Delta_2=4$, $\delta_a=1$, and $z_w=0.1$. The velocity V and β are, respectively, equal to $-0.1, 0.1$ (a); $-0.25, 0.25$ (b); and $-0.5, 0.5$ (c). Shown on the vertical axis is the intensity $|U_n|^2$.

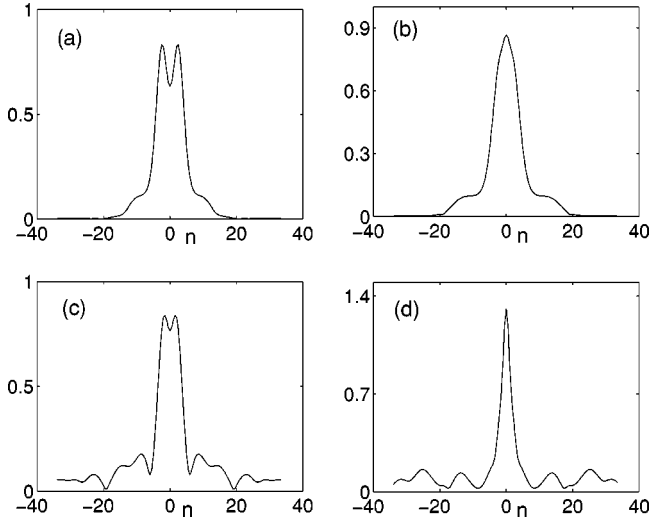


FIG. 17. Snapshot showing the evolution stages of the collision illustrated in Fig. 16(a).

light the similarity and differences between “classical” scalar discrete solitons and diffraction managed solitons. Figure 16 illustrates different possible interactions for which the two colliding beams are identical and move in opposite directions with identical speed. For small relative velocity the two colliding beams fuse and form a new state that is characterized by a localized core and oscillating tail. When propagating along the z direction, the core starts to develop double-hump pattern and becomes wider. As a result of an instability, the core beam reshapes itself into a Gaussian-like form and becomes narrower as more radiation is emitted (see Fig. 17). This behavior repeats and represents a “periodic” diffraction managed analog of the fused “classical” case [compare with Fig. 13(a)]. For higher velocities, the two beams cross each others trajectory. The outgoing traveling waves are characterized by modulated envelopes. The higher the collision velocity the larger the modulation amplitude. This behavior is similar to the one observed with “classical” soliton [compare with Figs. 13(b), 13(c)].

D. Vector interaction: Diffraction management

Next, we investigate what happens in the vector case, when the two beams interact via the cross-phase coupling. Figure 18 depicts different soliton collision scenarios for various values of η but fixed soliton velocities. In other words, the mode U_n is always stationary while V_n moves with fixed velocity $V = -0.1$ and the only parameter we change is η . It turns out that interactions between discrete diffraction-managed solitons differ fundamentally from their “classical” counterparts, as can be seen from Fig. 18 (see, for example, Fig. 14). For small value of $\eta = 0.1$ the interaction results in a fascinating process. Immediately after the collision, the two modes partially pass each other [see Figs. 19(a), 19(b)] and then, as a result of an attractive force, both beams turn over and come back to the initial state. Instead of continuing to go away from each other the two polarization modes turn back again. This behavior persists for very long distances and demonstrate a bound state recurrence-like phenomena.

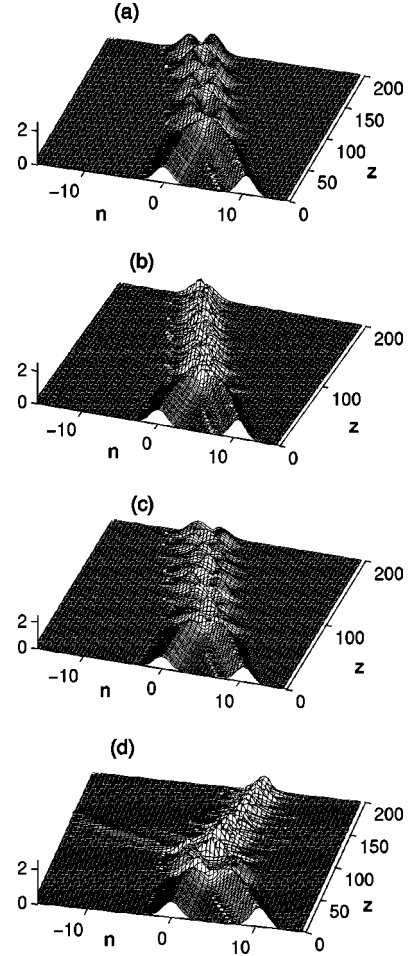


FIG. 18. Interaction between diffraction managed vector solitons for different values of cross-phase modulation coefficient (η) obtained by a direct numerical simulation of Eq. (5) evaluated at each map period. Shown on the vertical axis is the intensity (vertical axis) of the two colliding beams $I_n = |U_n|^2 + |V_n|^2$. Before collision, U_n is the stationary beam on the left and V_n is the mode on the right that travels with velocity V . Parameters are $\omega = 1$, $h = 0.5$, $s = 1$, $\Delta_1 = -\Delta_2 = 4$, $\delta_a = 1$, and $z_w = 0.1$. The velocity $V = -0.1$ and $\beta = 0.1$ with η equal to 0.1 (a), $2/3$ (b), 1 (c), and 2 (d).

Increasing the value of η to $2/3$ changes the interaction picture as more radiation is emitted and the resulting collision products exhibit multihump structure and constantly change their relative position. When the interaction takes place, the U_n (dashed line) intensity has a double-humped profile while V_n (solid line) is single humped [see Figs. 20(a), 20(b)]. After propagating for some distance, then exactly the opposite happens. Now the intensity of the V_n polarization is double-humped whereas U_n has a single hump. When the cross- and self-phase modulation coefficients are identical then the collision product is a bound state composed of single- and double-humped intensity profiles. Upon propagation, this bound state hops to the right and left, back and forth in a periodic manner [see Figs. 21(a), 21(b)]. Monitoring the evolution of the V_n mode shows that its double hump structure (in intensity) is preserved but exhibits an “internal” dynamics, i.e., the distance between the first and second maximum changes with z . In all of the above cases,

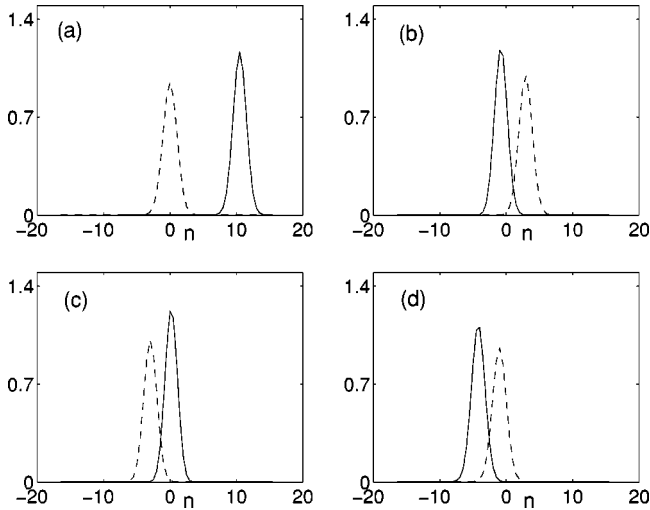


FIG. 19. Snapshot showing the evolution stages of the collision illustrated in Fig. 18(a). Dashed (solid) lines depicts $|U_n|^2$ ($|V_n|^2$). (a) is the initial condition and (b)–(d) shows interactions at different increasing distances from $z=0$, respectively.

the resulting beam moves with a negative velocity. Interestingly, for $\eta=2$, the collision process results in a “fused” travelinglike wave that moves in the positive direction with an additional small residual beam that propagates in the negative direction [Fig. 18(d)]. This fused state evolved from an intricate process. After collision, the intensities of both polarizations develop multihump structures [Fig. 22(a)], which decay as a result of instability and form two lumps together with a side wave [Fig. 22(b)]. This residual wave escapes away from the center and, as a result, both U_n and V_n relax into a “fused” state [Figs. 22(c), 22(d)] with emission of additional radiation.

VIII. CONCLUSIONS

In this paper we have investigated scalar and vector discrete diffraction managed systems. We have compared the

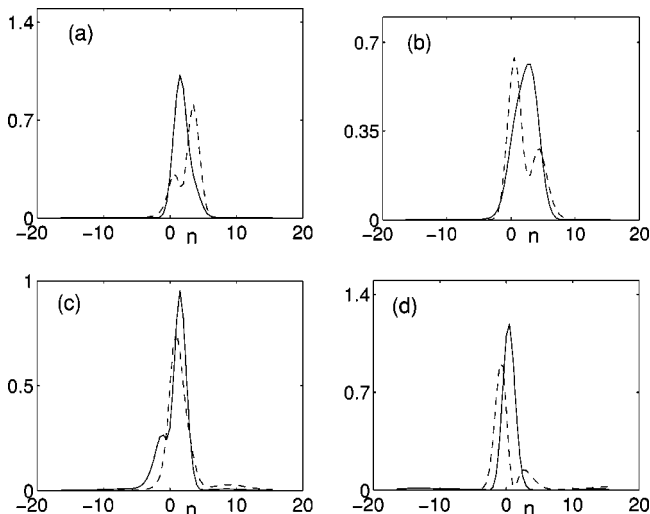


FIG. 20. Snapshot showing the evolution stages of the collision illustrated in Fig. 18(b). Dashed (solid) lines depict $|U_n|^2$ ($|V_n|^2$).

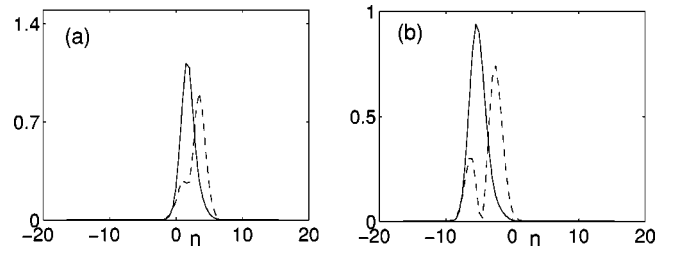


FIG. 21. Snapshot showing the intensity profile of both modes, $|U_n|^2$ (dashed) and $|V_n|^2$ (solid) right after the collision (a) and the last computational stage of the collision (b). These snapshots correspond to Fig. 18(c).

diffraction managed cases with their “classical” counterparts. The proposed vector model describes propagation of two polarization modes interacting in a waveguide array with Kerr nonlinearity in the presence of varying diffraction. The coupling of the two fields is described via the cross-phase modulation coefficient. In the limit of strong diffraction management we derive averaged equations governing the slow dynamics of the beam’s amplitudes and stationary (in the form of bright-bright vector bound state) as well as “approximate” traveling wave solutions are obtained. Through an extensive series of direct numerical simulations, we study interactions between periodic diffraction-managed solitons for different values of velocities, diffraction, and cross-phase modulation coefficients. In both the scalar and vector cases, we find that the interaction picture involves beam shaping, fusion, fission, nearly elastic collision, and, in some cases, multihump structures.

ACKNOWLEDGMENTS

M.J.A. was partially supported by the Air Force Office of Scientific Research under Grant No. F49620-00-1-0031 and by the NSF under Grant No. DMS-0070792. Z.H.M. would like to thank the Rothschild Foundation for financial support.

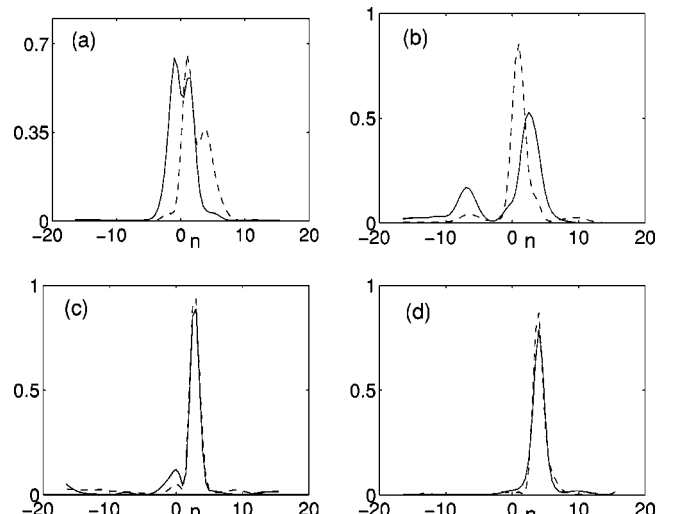


FIG. 22. Snapshot showing the evolution stages of the collision illustrated in Fig. 18(d). Dashed (solid) lines depict $|U_n|^2$ ($|V_n|^2$).

- [1] D. Henning and G.P. Tsironis, *Phys. Rep.* **307**, 333 (1999); O.M. Braun and Y.S. Kivshar, *ibid.* **306**, 1 (1998); S. Flach and C.R. Willis, *ibid.* **295**, 181 (1998); F. Lederer and J.S. Aitchison, in *Proceedings of the Les Houches Workshop on Optical Solitons*, edited by V.E. Zakharov and S. Wabnitz (Springer-Verlag, Berlin, 1999).
- [2] D.N. Christodoulides and R.J. Joseph, *Opt. Lett.* **13**, 794 (1988).
- [3] Y.S. Kivshar, *Opt. Lett.* **18**, 1147 (1993); W. Krolikowski and Y.S. Kivshar, *J. Opt. Soc. Am. B* **13**, 876 (1996).
- [4] A.B. Aceves, C. De Angelis, S. Trillo, and S. Wabnitz, *Opt. Lett.* **19**, 332 (1994); A.B. Aceves, C. De Angelis, T. Peschel, R. Muschall, F. Lederer, S. Trillo, and S. Wabnitz, *Phys. Rev. E* **53**, 1172 (1996); A.B. Aceves, C. De Angelis, A.M. Rubenchik, and S.K. Turitsyn, *Opt. Lett.* **19**, 329 (1994).
- [5] F. Lederer, S. Darmanyan, and A. Kobayakov, in *Spatial Solitons*, edited by S. Trillo and W. Torruellas (Springer-Verlag, Berlin, 2001), pp. 267–290; P.G. Kevrekidis, K.Ø. Rasmussen, and A.R. Bishop, *Int. J. Mod. Phys. B* **15**, 2833 (2001).
- [6] T. Peschel, U. Peschel, and F. Lederer, *Phys. Rev. E* **57**, 1127 (1998).
- [7] S. Darmanyan, A. Kobayakov, and F. Lederer, *Phys. Rev. E* **57**, 2344 (1998).
- [8] H. Eisenberg, Y. Silberberg, R. Morandotti, A. Boyd, and J. Aitchison, *Phys. Rev. Lett.* **81**, 3383 (1998).
- [9] R. Morandotti, U. Peschel, J. Aitchison, H. Eisenberg, and Y. Silberberg, *Phys. Rev. Lett.* **83**, 2726 (1999).
- [10] R. Morandotti, U. Peschel, J. Aitchison, H. Eisenberg, and Y. Silberberg, *Phys. Rev. Lett.* **83**, 4756 (1999).
- [11] T. Pertsch, P. Dannberg, W. Elflein, A. Bräuer, and F. Lederer, *Phys. Rev. Lett.* **83**, 4752 (1999).
- [12] G. Lenz, I. Talanina, and C. Martijn de Sterke, *Phys. Rev. Lett.* **83**, 963 (1999).
- [13] H. Eisenberg, Y. Silberberg, R. Morandotti, and J. Aitchison, *Phys. Rev. Lett.* **85**, 1863 (2000).
- [14] R. Morandotti, H. Eisenberg, Y. Silberberg, M. Sorel, and J. Aitchison, *Phys. Rev. Lett.* **86**, 3296 (2001).
- [15] M.J. Ablowitz and Z.H. Musslimani, *Phys. Rev. Lett.* **87**, 254102 (2001).
- [16] S.F. Mingaleev, and Y.S. Kivshar, *Phys. Rev. Lett.* **86**, 5474 (2001); A.A. Sukhorukov and Y.S. Kivshar, *ibid.* **87**, 083901 (2001); *Phys. Rev. E* **65**, 036609 (2002).
- [17] A. Trombettoni and A. Smerzi, *Phys. Rev. Lett.* **86**, 2353 (2001).
- [18] D.N. Christodoulides and E.D. Eugenieva, *Phys. Rev. Lett.* **87**, 233901 (2001); *Opt. Lett.* **26**, 1876 (2001); E.D. Eugenieva, N.K. Efremidis, and D.N. Christodoulides, *ibid.* **26**, 1978 (2001); *Opt. Photonics News* **12**, 57 (2001).
- [19] A. Yariv, *Optical Electronics*, 5th ed. (Oxford University Press, New York, 1997).
- [20] S. Darmanyan, A. Kobayakov, E. Schmidt, and F. Lederer, *Phys. Rev. E* **57**, 3520 (1998).
- [21] S. Somekh, E. Garmire, A. Yariv, H.L. Garvin, and R.G. Hunsperger, *Appl. Phys. Lett.* **22**, 46 (1973).
- [22] V.I. Petviashvili, *Sov. J. Plasma Phys.* **2**, 257 (1976).
- [23] M.J. Ablowitz and G. Biondini, *Opt. Lett.* **23**, 1668 (1998).
- [24] M.J. Ablowitz, Z. H. Musslimani, and G. Biondini, *Phys. Rev. E* (to be published).
- [25] M.J. Ablowitz, Y. Ohta, and D. Trubatch, *Phys. Lett. A* **253**, 287 (1999).
- [26] M.J. Ablowitz, B. Prinari, and D. Trubatch, APPM Report No. 473, Department of Applied Mathematics, University of Colorado at Boulder, 2001 (unpublished).
- [27] I.R. Gabitov and S.K. Turitsyn, *Opt. Lett.* **21**, 327 (1996).
- [28] S.K. Turitsyn, *Sov. Phys. JETP Lett.* **65**, 845 (1997).
- [29] J.H.B. Nijhof, W. Forysiak, and N.J. Doran, *IEEE J. Sel. Top. Quantum Electron.* **6**, 330 (2000).
- [30] In close analogy to the definition of a chirp in dispersion managed solitons, here, the chirp of a discrete beam $\Phi_n(z) = |\Phi_n(z)|\exp[i\Theta_n(z)]$ is defined to be the coefficient of n^2 in the expansion of $\Theta_n(z)$ in a “Taylor series” around $n=0$. In other words, if $\Theta_n(z) \approx c_0(z) + c_1(z)n + c_2(z)n^2 + \dots$, then the chirp is given by $c_2(z)$. This definition is valid for moderately localized solitons and breaks down for strongly localized beams.
- [31] H. Feddersen, *Lecture Notes in Physics Vol. 393* (Springer, Berlin, 1991), p. 159.
- [32] D.B. Duncan, J.C. Eilbeck, H. Feddersen, and J.A.D. Wattis, *Physica D* **68**, 1 (1993).
- [33] S. Flach and K. Kladko, *Physica D* **127**, 61 (1999).
- [34] S. Flach, Y. Zolotaryuk, and K. Kladko, *Phys. Rev. E* **59**, 6105 (1999).
- [35] S. Aubry and T. Cretegny, *Physica D* **119**, 34 (1998).
- [36] Ch. Claude, Y.S. Kivshar, O. Kluth, and K.H. Spatschek, *Phys. Rev. B* **47**, 14 228 (1993).